Journal of Sound and Vibration (2001) **246**(4), 625–652
doi:10.1006/jsvi.2001.3690, available online at http://www.idealibrary.com on IDEAL®

EXPLICIT PREDICTOR–MULTICORRECTOR TIME DISCONTINUOUS GALERKIN METHODS FOR LINEAR DYNAMICS

A. Bonelli and O. S. Bursi

Dipartimento di Ingegneria Meccanica e Strutturale, Università di Trento, 38050 *Trento, Italy*.
E-mail: *alessio.bonelli@ing.unitn.it*

and

M. Mancuso

Dipartimento di Scienze dell'Ingegneria, Università di Modena e Reggio Emilia, 41100 *Modena, Italy*

(*Received* 22 *September* 2000, *and in final form* 5 *February* 2001)

This paper focuses on the formulation and implementation of explicit predictor–multicorrector Time Discontinuous Galerkin methods for linear structural dynamics. The formulation of the schemes is based on piecewise linear functions in time that approximate displacements and momenta. Both the predictors and correctors are designed to inherit third order accuracy from the exact parent implicit Time Discontinuous Galerkin method. Moreover, they are endowed with large stability limits and controllable numerical dissipation by means of an algorithmic parameter. Thereby, the resulting algorithms appear to be competitive with standard explicit algorithms for structural dynamics. Representative numerical simulations are presented illustrating the performance of the proposed numerical schemes and confirming the analytical results.

© 2001 Academic Press

1. INTRODUCTION

The common approach towards the numerical solution of structural dynamic problems is, first, to discretize the spatial domain, which results in a system of coupled second order ordinary differential equations with time as an independent variable. In order to solve this initial value problem, implicit and explicit time integration procedures based on finite difference methods are widely used. Implicit methods need factorization of the effective stiffness (or effective mass) matrix and, thereby, a certain computational effort is required. Since they can be unconditionally stable, large time steps can be employed. Conversely, explicit algorithms typically avoid matrix factorization when a diagonal mass matrix is used, thus requiring much less storage and computational effort per time step. However, their conditional stability imposes a time-step size restriction to ensure numerical stability. For this reason, they are used in wave propagation problems, where the time-step size needed for accuracy is of the same order of the stability limit step size [1].

Although several explicit algorithms with high-accuracy order have been proposed (such as Katona and Zienkiewicz [2] and Hoff and Taylor's methods [3]), the second order Central Difference method (CD) is still the most popular explicit scheme [1, p. 495]. As a matter of fact, higher order explicit methods need higher derivative terms and thereby, more computational effort and additional storage is required.

0022-460X/01/390625 + 28 $35.00/0 © 2001 Academic Press

The numerical time integration of a semidiscrete problem may present non-physical oscillations, which are related to spurious high-frequency modes introduced by the spatial discretization [1, p. 498]. As the CD method does not introduce any algorithmic damping, it may exhibit unwanted behaviour owing to the accurate integration of spurious modes. In order to avoid these effects, algorithmic dissipation in the high-frequency modes should be introduced. As a result, explicit finite-difference-based methods designed to attenuate high-frequency oscillation modes were conceived (see reference [4] and references therein).

A recent alternative approach to the numerical time integration of structural systems is based on Galerkin formulations in the time domain [5–8]. Whilst the space is discretized using conventional finite elements, the time interval is partitioned in a number of subintervals, where the response is approximated by means of trial functions in the time variable. The use of discontinuous displacement and momentum fields leads to the class of implicit schemes named Time Discontinuous Galerkin (TDG) methods. Higher order unconditionally stable algorithms are obtained, by which any undesirable high-frequency mode can be damped out without introducing excessive algorithmic damping in the low-frequency response. However, these methods require the factorization of a matrix larger than the one exploited in standard implicit schemes owing to the unknown extra displacement and momentum fields. Thereby, added computational effort is required. In order to obviate this problem, Li and Wiberg [9] implemented a predictor–multicorrector solution algorithm in the TDG method. More specifically, the algorithm requires a factorization of a reduced matrix for each fixed time-step size and few iterations for solving the resulting system of coupled equations in the unknown velocities. Based on a similar strategy, the same authors proposed TDG methods based on an explicit time integration [10, 11]. The resulting explicit scheme was third order accurate and endowed with a stability limit higher than that of the CD method. Nonetheless, aspects related to the control of the algorithmic dissipation were not investigated.

In this paper, a new class of explicit predictor–multicorrector step-by-step integration algorithms is presented, based on the implicit TDG scheme with linear trial and weighting functions in time. The resulting algorithms are third order accurate and their stability limit is higher than the one exhibited by the CD method. Moreover, in contrast with the aforementioned explicit TDG-based schemes, the proposed algorithms are endowed with a user-controllable algorithmic dissipation. In contrast to traditional dissipative finite difference methods, these schemes do not reduce in accuracy when stronger dissipation is required and do not need the computation of the time derivative of the acceleration. As a result, they are competitive when medium-term high-quality numerical computations are performed.

The remainder of the paper is organized as follows. In section 2 the formulation of the implicit TDG method is presented. In section 3, the new class of explicit schemes is derived. Section 4 presents the accuracy and stability analysis of the methods. Section 5 describes numerical experiments which demonstrate the properties of the schemes predicted from theoretical analyses. In addition, some comparisons with numerical results obtained by other commonly used time integrators are presented whilst conclusions are drawn in section 6. Finally, some details concerning an alternative implementation of the proposed methods are discussed in Appendix A.

2. FORMULATION OF THE IMPLICIT TDG METHOD

Since the main focus of the paper is the study of certain time-step algorithms, the semidiscrete initial value problem is considered. It reads as

$$\mathbf{M}\ddot{\mathbf{q}}(t) + \mathbf{C}\dot{\mathbf{q}}(t) + \mathbf{K}\mathbf{q}(t) = \mathbf{f}(t), \quad t \in I = (0, T),$$

$$\mathbf{q}(0) = \bar{\mathbf{q}}_0, \tag{1}$$

$$\dot{\mathbf{q}}(0) = \bar{\mathbf{v}}_0,$$

where $\mathbf{q}(t)$ is the vector of displacement parameters arising from a spatial discretization. $\mathbf{M}$ is the symmetric positive-definite mass matrix, $\mathbf{C}$ the viscous damping matrix, $\mathbf{K}$ the stiffness matrix, $\mathbf{f}(t)$ the vector of applied forces and I defines the time domain. The superposed dots indicate differentiation with respect to time t. Equations (1) are obtained by means of standard finite element procedures (for example, see reference [1]).

Initial value problem (1) can be rewritten in the first order form

$$\dot{\mathbf{p}}(t) + \mathbf{C}\mathbf{M}^{-1}\mathbf{p}(t) + \mathbf{K}\mathbf{q}(t) = \mathbf{f}(t), \quad t \in I = (0, T),$$

$$\mathbf{M}^{-1}\mathbf{p}(t) - \dot{\mathbf{q}}(t) = 0, \quad t \in I = (0, T),$$

$$\mathbf{q}(0) = \bar{\mathbf{q}}_0,$$

$$\mathbf{p}(0) = \bar{\mathbf{p}}_0 = \mathbf{M}\bar{\mathbf{v}}_0, \tag{2}$$

where $\mathbf{p}(t)$ are the momenta. The TDG methods are derived from a weighted residual formulation of equations (2), with the initial conditions enforced in a weak manner.

In this paper, the formulation with piecewise linear time interpolants of displacements and momenta is adopted. The corresponding time-step method will be referred to as TDG1 method. Consider a partition of the time domain

$$I_i = (t_i, t_{i+1}), \quad i = 0, \ldots, N, \tag{3}$$

where $0 = t_0 < t_1 < \cdots < t_N = T$ and $\Delta t = t_{i+1} - t_i$ is the time-step size. The following notation is convenient hereafter

$$t_i^- = \lim_{t \to t_i^-} t,$$

$$t_i^+ = \lim_{t \to t_i^+} t. \tag{4}$$

Let $(\mathbf{q}_0, \mathbf{p}_0)$ denote the vectors of displacements and momenta, respectively, at t_i^-, which are known from either the previous step calculation or the initial data ($\bar{\mathbf{q}}_0$ and $\bar{\mathbf{p}}_0$) if $i = 0$. Moreover, let $(\mathbf{q}_1, \mathbf{p}_1)$ and $(\mathbf{q}_2, \mathbf{p}_2)$ denote the displacements and momenta at t_i^+ and t_{i+1}^-, respectively. These quantities are illustrated schematically in Figure 1. The displacements and momenta at time $t \in I_i$ are represented as follows:

$$\mathbf{q}(t) = t_1(t)\mathbf{q}_1 + t_2(t)\mathbf{q}_2,$$

$$\mathbf{p}(t) = t_1(t)\mathbf{p}_1 + t_2(t)\mathbf{p}_2, \tag{5}$$

where

$$t_1(t) = \frac{t_{i+1} - t}{\Delta t},$$

$$t_2(t) = \frac{t - t_i}{\Delta t}. \tag{6}$$

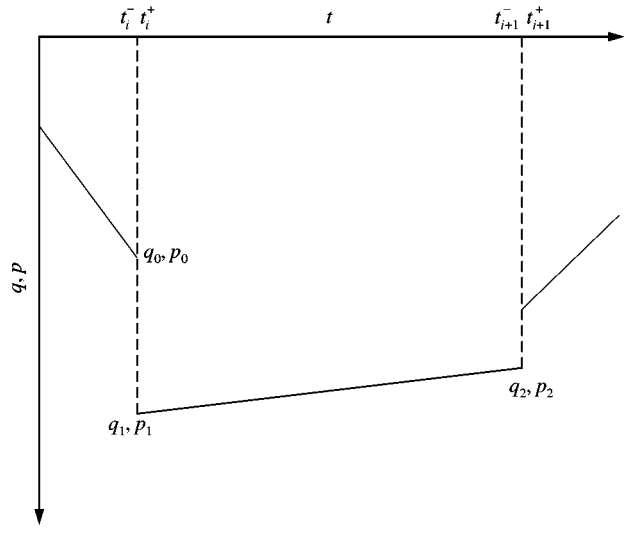

Figure 1. Time-finite elements with linear trial functions.

The corresponding weighting functions are

$$\mathbf{w}_{\mathbf{q}}(t) = t_1(t)\mathbf{w}_{\mathbf{q}_1} + t_2(t)\mathbf{w}_{\mathbf{q}_2},$$

$$\mathbf{w}_{\mathbf{p}}(t) = t_1(t)\mathbf{w}_{\mathbf{p}_1} + t_2(t)\mathbf{w}_{\mathbf{p}_2}. \tag{7}$$

From this notation, the TDG1 method is obtained by enforcing the weighted residual form of equations (2): find $\mathbf{q}_1$, $\mathbf{q}_2$, $\mathbf{p}_1$ and $\mathbf{p}_2$ such that

$$\int_{I_i} \mathbf{w}_{\mathbf{q}}^{\mathrm{T}}(\dot{\mathbf{p}} + \mathbf{C}\mathbf{M}^{-1}\mathbf{p} + \mathbf{K}\mathbf{q} - \mathbf{f})\,\mathrm{d}t + \int_{I_i} \mathbf{w}_{\mathbf{p}}^{\mathrm{T}}(\mathbf{M}^{-1}\mathbf{p} - \dot{\mathbf{q}})\,\mathrm{d}t$$

$$- \mathbf{w}_{\mathbf{p}}^{\mathrm{T}}(t_i^+)(\mathbf{q}(t_i^+) - \mathbf{q}_0) + \mathbf{w}_{\mathbf{q}}^{\mathrm{T}}(t_i^+)(\mathbf{p}(t_i^+) - \mathbf{p}_0) = 0, \tag{8}$$

for all $\mathbf{w}_{\mathbf{q}_1}$, $\mathbf{w}_{\mathbf{q}_2}$, $\mathbf{w}_{\mathbf{p}_1}$, $\mathbf{w}_{\mathbf{p}_2}$. Substituting equations (5) and the weighting functions into equation (8), the following algebraic system is obtained:

$$\begin{aligned}
&\text{a)}\quad \frac{\Delta t}{3}\mathbf{K}\left(\mathbf{q}_1 + \frac{1}{2}\,\mathbf{q}_2\right) + \left(\frac{1}{2}\mathbf{I} + \frac{\Delta t}{3}\mathbf{C}\mathbf{M}^{-1}\right)\mathbf{p}_1 + \left(\frac{1}{2}\mathbf{I} + \frac{\Delta t}{6}\mathbf{C}\mathbf{M}^{-1}\right)\mathbf{p}_2 = \mathbf{p}_0 + \mathbf{F}_1,\\
&\text{b)}\quad \frac{\Delta t}{3}\mathbf{K}\left(\frac{1}{2}\mathbf{q}_1 + \mathbf{q}_2\right) + \left(-\frac{1}{2}\mathbf{I} + \frac{\Delta t}{6}\mathbf{C}\mathbf{M}^{-1}\right)\mathbf{p}_1 + \left(\frac{1}{2}\mathbf{I} + \frac{\Delta t}{3}\mathbf{C}\mathbf{M}^{-1}\right)\mathbf{p}_2 = \mathbf{F}_2,\\
&\text{c)}\quad \frac{1}{2}(\mathbf{q}_1 + \mathbf{q}_2) - \frac{\Delta t}{3}\mathbf{M}^{-1}\left(\mathbf{p}_1 + \frac{1}{2}\mathbf{p}_2\right) = \mathbf{q}_0,\\
&\text{d)}\quad \frac{1}{2}(\mathbf{q}_1 - \mathbf{q}_2) + \frac{\Delta t}{3}\mathbf{M}^{-1}\left(\frac{1}{2}\mathbf{p}_1 + \mathbf{p}_2\right) = 0,
\end{aligned} \tag{9}$$

where

$$\mathbf{F}_1 = \int_{t_i}^{t_i+1} t_1(t)\,\mathbf{f}(t)\,\mathrm{d}t,$$

$$\mathbf{F}_2 = \int_{t_i}^{t_i+1} t_2(t)\,\mathbf{f}(t)\,\mathrm{d}t. \tag{10}$$

The TDG1 algorithm is third order accurate and L-stable, i.e., the high-frequency modes are nearly damped out in a single time step [6]. However, a drawback of the TDG1 method is related to the size of system (9), which is equal to $4 \cdot n_{DoF}$, where n_{DoF} is the number of degrees of freedom of the spatial discretization. This system is 4 times larger than those arising from conventional time discretizations of equation (1). Moreover, the coefficient matrix is non-symmetrical. Thereby, the development of suitable solution algorithms for equations (9) is a critical issue in the practical application of the method.

3. THE EXPLICIT PREDICTOR–MULTICORRECTOR METHOD

3.1. FORMULATION

In this section, an explicit method which inherits the third order accuracy and the dissipative properties of the implicit TDG method is proposed. In order to avoid an expensive explicit formulation, firstly, the computational effort related to the solution of system (9) has to be reduced. Therefore, an iterative predictor–multicorrector procedure is proposed [5, 11], where the number of correctors is limited to one or two. Moreover, the multicorrector phase relies on a solution in terms of displacements by means of a reduced iteration matrix. For simplicity, no damping is considered in equations (9). The extension to the damped case will be performed in section 3.3.

In order to reduce the computational effort related to the solution of equation (9), the unknown momenta $\mathbf{p}_1$ and $\mathbf{p}_2$ are eliminated from equation (9c, d), thus obtaining

$$\mathbf{x}_\mathbf{p} = \begin{bmatrix} \mathbf{p}_1 \\ \mathbf{p}_2 \end{bmatrix} = \begin{bmatrix} \dfrac{1}{\Delta t}\mathbf{M}(3\mathbf{q}_1 + \mathbf{q}_2 - 4\mathbf{q}_0) \\ \dfrac{1}{\Delta t}\mathbf{M}(-3\mathbf{q}_1 + \mathbf{q}_2 + 2\mathbf{q}_0) \end{bmatrix}. \tag{11}$$

Substituting relations (11) in equation (9a) and (9b) and multiplying equation (9b) by $-\frac{1}{3}$, the following system is obtained:

$$(\mathbf{B} + \mathbf{D})\,\mathbf{x}_\mathbf{q} - \mathbf{P}_0 = \mathbf{0} \tag{12}$$

for the undamped case, where

$$\mathbf{B} = \frac{1}{\Delta t}\begin{bmatrix} \mathbf{0} & \mathbf{M} \\ \mathbf{M} & \mathbf{0} \end{bmatrix}, \qquad \mathbf{D} = \begin{bmatrix} \dfrac{\Delta t}{3}\mathbf{K} & \dfrac{\Delta t}{6}\mathbf{K} \\ -\dfrac{\Delta t}{18}\mathbf{K} & -\dfrac{\Delta t}{9}\mathbf{K} \end{bmatrix},$$

$$\mathbf{x}_\mathbf{q} = \begin{bmatrix} \mathbf{q}_1 \\ \mathbf{q}_2 \end{bmatrix}, \qquad \mathbf{P}_0 = \begin{bmatrix} \mathbf{p}_0 + \dfrac{1}{\Delta t}\mathbf{M}\mathbf{q}_0 + \mathbf{F}_1 \\ \dfrac{1}{\Delta t}\mathbf{M}\mathbf{q}_0 - \dfrac{1}{3}\mathbf{F}_2 \end{bmatrix}. \tag{13}$$

Let $\mathbf{x}_q^{(k)}$ denote the kth trial value of the unknown displacements in a typical time step $[t_i, t_{i+1}]$. In order to advance from t_i to t_{i+1}, the following steps are performed.

3.1.1. *Predictor*

The predictor is designed to achieve the best accuracy and therefore it is expressed in terms of free parameters. It is based on the Taylor series expansion of the solution of the implicit parent algorithm

$$\mathbf{q}_1 = \mathbf{q}_0 - \frac{\Delta t^2}{6}\mathbf{M}^{-1}\dot{\mathbf{p}}_0 + \mathbf{O}(\Delta t^3),$$

$$\mathbf{q}_2 = \mathbf{q}_0 + \Delta t\mathbf{M}^{-1}\mathbf{p}_0 + \frac{\Delta t^2}{2}\mathbf{M}^{-1}\dot{\mathbf{p}}_0 + \mathbf{O}(\Delta t^3) \tag{14}$$

and on the discontinuity in time depicted in Figure 1 [10]. In equation (14), $\dot{\mathbf{p}}_0$ defines the time derivative of momenta evaluated at t_i^-, obtained from the equilibrium equation (2), namely

$$\dot{\mathbf{p}}_0 = \mathbf{f}(t_0) - \mathbf{K}\mathbf{q}_0. \tag{15}$$

In order to generalize equation (14) and setting $k = 0$ to initialize the unknowns, the following predictor is utilized:

$$\mathbf{q}_1^{(0)} = \mathbf{q}_0 + a\ \Delta t^2\mathbf{M}^{-1}\dot{\mathbf{p}}_0,$$

$$\mathbf{q}_2^{(0)} = \mathbf{q}_0 + \Delta t\mathbf{M}^{-1}\mathbf{p}_0 + b\ \Delta t^2\mathbf{M}^{-1}\dot{\mathbf{p}}_0 \tag{16}$$

where a and b are two free parameters. The vector $\dot{\mathbf{p}}_0$, defined in equation (15) could be also evaluated as derivative of momenta. However, this approach leads to unfavourable stability properties which are discussed at length in Appendix A.

3.1.2. *Corrector*

In order to solve system (12), an iterative scheme relying on displacement increments is used. If suffices to define a residual

$$\mathbf{r}^{(k)} = (\mathbf{B} + \mathbf{D})\,\mathbf{x}_\mathbf{q}^{(k)} - \mathbf{P}_0 \tag{17}$$

and a displacement increment

$$\Delta\mathbf{x}_\mathbf{q}^{(k)} = -[\mathbf{K}^*]^{-1}\mathbf{r}^{(k)}, \tag{18}$$

where $\mathbf{K}^*$ is

$$\mathbf{K}^* = \mathbf{B} \tag{19}$$

and $[\mathbf{K}^*]^{-1}$ exhibits the simple form

$$[\mathbf{K}^*]^{-1} = \mathbf{B}^{-1} = \Delta t\begin{bmatrix} \mathbf{0} & \mathbf{M}^{-1} \\ \mathbf{M}^{-1} & \mathbf{0} \end{bmatrix}. \tag{20}$$

The exact solution of system (12) would require $\mathbf{K}^* = \partial \mathbf{r}/\partial \mathbf{x}_\mathbf{q}|_{\mathbf{x}_\mathbf{q}^{(k)}} = \mathbf{B} + \mathbf{D}$. As a result, the proposed scheme neglects the stiffness contribution in equation (19). Hereafter, the new class of integration schemes is denoted as **E** methods. Three features of these algorithms contribute to the reduction of the computational effort: (i) the algorithms become explicit if a lumped mass matrix **M** is exploited in equation (20); (ii) the iteration matrix $\mathbf{K}^*$ is formed and factorized only once; and (iii) a maximum number of iterations k_{max} is prescribed. More specifically, E-1C defines the scheme which requires one corrector pass ($k_{max} = 1$) whilst the acronym E-2C stands for the method exploiting two corrector passes ($k_{max} = 2$).

3.2. IMPLEMENTATION

The solution procedure of the E schemes applied to linear structural dynamic problems follows.

1. Initial computations
   (a) Form both the diagonal mass matrix **M** and the stiffness matrix **K**.
   (b) Initialize $\mathbf{q}_0$, $\mathbf{p}_0$ and $\mathbf{f}(t_0)$.
   (c) Select the number of correctors k_{max} (1 or 2), the value of parameters a and b as well as the time-step size Δt.
2. For each time step ($i = 0, 1, \ldots, N-1$)
   (a) Compute the momenta time derivative at time t_i^-

$$\dot{\mathbf{p}}_i = \mathbf{f}(t_i) - \mathbf{K}\mathbf{q}_i.$$

   (b) Compute the vectors $\mathbf{P}_{i,1}$ and $\mathbf{P}_{i,2}$ (equation (13b)) on the basis of initial conditions and the external force

$$\mathbf{P}_{i,1} = \mathbf{p}_i + \frac{1}{\Delta t}\mathbf{M}\mathbf{q}_i + \int_{t_i}^{t_i+\Delta t} t_1(t)\,\mathbf{f}(t_i + t)\,\mathrm{d}t,$$

$$\mathbf{P}_{i,2} = \frac{1}{\Delta t}\mathbf{M}\mathbf{q}_i - \frac{1}{3}\int_{t_i}^{t_i+\Delta t} t_2(t)\,\mathbf{f}(t_i + t)\,\mathrm{d}t.$$

   (c) Set $k = 0$.
   (d) Compute the predictor displacements (equation (16)) at time t_i^+ and t_{i+1}^-

$$\mathbf{q}_1^{(0)} = \mathbf{q}_i + \Delta t^2\, a\, \mathbf{M}^{-1}\dot{\mathbf{p}}_i,$$

$$\mathbf{q}_2^{(0)} = \mathbf{q}_i + \Delta t \mathbf{M}^{-1}\mathbf{p}_i + \Delta t^2\, b\, \mathbf{M}^{-1}\dot{\mathbf{p}}_i.$$

   (e) Multicorrector

      i. Compute the residual vectors (equation (17))

$$\mathbf{r}_1^{(k)} = \frac{\Delta t}{3}\mathbf{K}\mathbf{q}_1^{(k)} + \left(\frac{1}{\Delta t}\mathbf{M} + \frac{\Delta t}{6}\mathbf{K}\right)\mathbf{q}_2^{(k)} - \mathbf{P}_{i,1},$$

$$\mathbf{r}_2^{(k)} = \left(\frac{1}{\Delta t}\mathbf{M} - \frac{\Delta t}{18}\mathbf{K}\right)\mathbf{q}_1^{(k)} - \frac{\Delta t}{9}\mathbf{K}\mathbf{q}_2^{(k)} - \mathbf{P}_{i,2}.$$

ii. Compute the displacement increments (equation (18))

$$\Delta \mathbf{q}_1^{(k)} = \Delta t \mathbf{M}^{-1} \mathbf{r}_2^{(k)},$$

$$\Delta \mathbf{q}_2^{(k)} = \Delta t \mathbf{M}^{-1} \mathbf{r}_1^{(k)}.$$

iii. Compute the displacement vectors

$$\mathbf{q}_1^{(k+1)} = \mathbf{q}_1^{(k)} + \Delta \mathbf{q}_1^{(k)},$$

$$\mathbf{q}_2^{(k+1)} = \mathbf{q}_2^{(k)} + \Delta \mathbf{q}_2^{(k)}.$$

iv. $k = k + 1$.

v. If $k < k_{max}$ go to *i*.

(f) Compute the displacement vector at time $t_{i+1} = t_i + \Delta t$

$$\mathbf{q}_{i+1} = \mathbf{q}_2^{(k)}.$$

(g) Compute the momentum vector (equation (11)) at time $t_{i+1} = t_i + \Delta t$

$$\mathbf{p}_{i+1} = \frac{1}{\Delta t} \mathbf{M}(-3\mathbf{q}_1^{(k)} + \mathbf{q}_2^{(k)} + 2\mathbf{q}_i).$$

(h) $i = i + 1$.

(i) If $i < N$ go to (a).

The parameters a and b are chosen to obtain third order accuracy and controllable dissipative properties. These issues are discussed at length in section 4.

3.3. THE TDG EXPLICIT METHOD FOR DAMPED SYSTEMS

The formulation presented so far can be extended easily to systems with physical damping. In these conditions, equation (12) reads

$$(\mathbf{B} + \mathbf{V} + \mathbf{D})\,\mathbf{x}_\mathbf{q} - \mathbf{P}_0 = \mathbf{0}, \tag{21}$$

where

$$\mathbf{V} = \begin{bmatrix} \frac{1}{2}\mathbf{C} & \frac{1}{2}\mathbf{C} \\ -\frac{1}{2}\mathbf{C} & \frac{1}{2}\mathbf{C} \end{bmatrix}. \tag{22}$$

In several explicit algorithms, the damping can be dealt with either implicitly or explicitly [4]. Both choices are available for the proposed schemes for which residual (17) reads

$$\mathbf{r}^{(k)} = (\mathbf{B} + \mathbf{V} + \mathbf{D})\,\mathbf{x}_\mathbf{q}^{(k)} - \mathbf{P}_0. \tag{23}$$

In the former case, $\mathbf{K}^* = \mathbf{B} + \mathbf{V}$ in equation (18). If $\mathbf{C}$ is a non-diagonal matrix, the methods become implicit [4, 12]. In the latter case, $\mathbf{K}^*$ is still defined through relation (19) and thereby, purely explicit schemes can be obtained.

4. ACCURACY AND STABILITY ANALYSIS

In this section, consistency and stability properties of the proposed predictor–multicorrector algorithms are examined. Since a multiple-degrees-of-freedom coupled system can be decomposed into n_{DoF} uncoupled scalar equations in the linear regime, it suffices to perform the analysis of an algorithm on a single-degree-of-freedom model equation [1, p. 492]. In these conditions, the matrices in equation (1) becomes scalar and the vector $\mathbf{x}_\mathbf{q}$ in equation (13c) collects only two components.

Introducing the natural frequency

$$\omega = \sqrt{\frac{k}{m}} \tag{24}$$

equation (1) for an undamped system can be written as

$$\ddot{q}(t) = \omega^2 q(t) = \frac{f(t)}{m}. \tag{25}$$

Thereby, the predictor defined in equation (16) becomes

$$q_1^{(0)} = q_0 + \Delta t^2 a \frac{\dot{p}_0}{m},$$

$$q_2^{(0)} = q_0 + \Delta t \frac{p_0}{m} + \Delta t^2 b \frac{\dot{p}_0}{m}, \tag{26}$$

where

$$\dot{p}_0 = f(0) - m\omega^2 q_0. \tag{27}$$

4.1. ITERATION MATRIX

Combining equation (17) with equations (18) and (19), gives

$$\mathbf{x}_\mathbf{q}^{(k+1)} = -\mathbf{B}^{-1}\mathbf{D}\mathbf{x}_\mathbf{q}^{(k)} + \mathbf{B}^{-1}\mathbf{P}_0 \tag{28}$$

which can be expressed in the compact form

$$\mathbf{x}_\mathbf{q}^{(k+1)} = \mathbf{A}_{IT}\mathbf{x}_\mathbf{q}^{(k)} + \mathbf{g}, \tag{29}$$

where $\mathbf{A}_{IT} = -\mathbf{B}^{-1}\mathbf{D}$ is the so-called iteration matrix and $\mathbf{g} = \mathbf{B}^{-1}\mathbf{P}_0$. Thus

$$\mathbf{A}_{IT} = \begin{bmatrix} \frac{1}{18}\Omega^2 & \frac{1}{9}\Omega^2 \\ -\frac{1}{3}\Omega^2 & -\frac{1}{6}\Omega^2 \end{bmatrix},$$

$$\mathbf{g} = \begin{bmatrix} q_0 - \frac{1}{2}\frac{\Delta t}{m}F_2 \\ q_0 + \frac{\Delta t}{m}p_0 + \frac{\Delta t}{m}F_1 \end{bmatrix}, \tag{30}$$

where

$$\Omega = \omega \Delta t \tag{31}$$

is the non-dimensional frequency. In this case, $\mathbf{A}_{IT}$ has complex conjugate eigenvalues. Given an arbitrary initial vector $\mathbf{x}_{\mathbf{q}}^{(0)}$, a necessary and sufficient condition for the process defined in equation (29) to converge to the exact solution of the algebraic problem (12) is

$$\rho(\mathbf{A}_{IT}) < 1, \tag{32}$$

where $\rho(\mathbf{A}_{IT})$ denotes the spectral radius of the matrix $\mathbf{A}_{IT}$ [13, p. 7]. As a result, the convergence condition is

$$\rho(\mathbf{A}_{IT}) = \tfrac{1}{6}\Omega^2 < 1 \Rightarrow \Omega < \sqrt{6} \tag{33}$$

which can be considered as a stability condition of the explicit scheme. Thus, at convergence, the stability limit of the method is higher than the one exhibited by the CD method. It should be recalled that only one or two iterations are performed in the proposed schemes leading to approximate solutions provided by equation (29). As a result, the stability limits can be different from that provided by equation (33).

The explicit method proposed by Wiberg and Li [10] entails the same iteration matrix $\mathbf{A}_{IT}$ as that defined in equation (30a); nonetheless, their algorithm has been formulated in terms of velocities.

4.2. AMPLIFICATION MATRIX

Consider the recursive form of the E method

$$\mathbf{y}_1 = \mathbf{A}\,\mathbf{y}_0 + \mathbf{L}_0, \tag{34}$$

where

$$\mathbf{y}_0 = \begin{bmatrix} q_0 \\ p_0 \end{bmatrix}, \qquad \mathbf{y}_1 \begin{bmatrix} q_2 \\ p_2 \end{bmatrix} \tag{35}$$

according to Figure 1. $\mathbf{A}$ defines the amplification matrix and $\mathbf{L}$ is the load vector which depends on the external forces. Consistency and stability of a time-step algorithm can be analyzed through the spectral approach [1, p. 492], where the unforced case ($f = 0$) can be considered.

The amplification matrix $\mathbf{A}$ can be expressed in terms of the predictor defined in equation (16), the iteration matrix $\mathbf{A}_{IT}$ and the vector $\mathbf{g}$ defined in equation (30a, b) respectively. As the vector $\mathbf{g}$ depends on the initial conditions only, it can be written as

$$\mathbf{g} = \mathbf{G}\mathbf{y}_0, \tag{36}$$

where

$$\mathbf{G} = \begin{bmatrix} 1 & 0 \\ 1 & \dfrac{\Delta t}{m} \end{bmatrix}. \tag{37}$$

Moreover, the predictor defined in equation (26) is employed to initialize the iterative process (29)

$$\mathbf{x}_{\mathbf{q}}^{(0)} = \begin{bmatrix} q_1^{(0)} \\ q_2^{(0)} \end{bmatrix} = \mathbf{E}\mathbf{y}_0, \tag{38}$$

where the matrix

$$\mathbf{E} = \begin{bmatrix} 1 - \Delta t^2 a\omega^2 & 0 \\ 1 - \Delta t^2 b\omega^2 & \dfrac{\Delta t}{m} \end{bmatrix} \tag{39}$$

depends on the free parameters a and b. The unknown displacements $\mathbf{x}_{\mathbf{q}}$ are obtained performing k_{max} (1 or 2) correctors. By means of the iteration matrix $\mathbf{A}_{IT}$, it is straightforward to show that

$$\begin{aligned} \mathbf{x}_{\mathbf{q}}^{(k_{max})} &= \mathbf{A}_{IT}^{k_{max}} \mathbf{x}_{\mathbf{q}}^{(0)} + \sum_{i=1}^{k_{max}-1} \mathbf{A}_{IT}^{i} \mathbf{g} + \mathbf{g} \\ &= \mathbf{A}_{IT}^{k_{max}} \mathbf{E}\mathbf{y}_0 + \sum_{i=1}^{k_{max}-1} \mathbf{A}_{IT}^{i} \mathbf{G}\mathbf{y}_0 + \mathbf{G}\mathbf{y}_0 \\ &= \mathbf{Q}\mathbf{y}_0, \end{aligned} \tag{40}$$

where

$$\mathbf{Q} = \left[\mathbf{A}_{IT}^{k_{max}} \mathbf{E} + \left(\mathbf{I} + \sum_{i=1}^{k_{max}-1} \mathbf{A}_{IT}^{i} \right) \mathbf{G} \right]. \tag{41}$$

Once $\mathbf{x}_{\mathbf{q}}^{(k_{max})}$ is obtained from equation (40), the momenta at t_{i+1}^{-} can be evaluated through equation (11b), i.e.

$$\begin{aligned} p_2 &= -\frac{3}{\Delta t} m q_1 + \frac{1}{\Delta t} m q_2 + \frac{2}{\Delta t} m q_0 \\ &= \mathbf{W}_1 \mathbf{y}_0 + \mathbf{W}_2 \mathbf{x}_q = (\mathbf{W}_1 + \mathbf{W}_2 \mathbf{Q}) \mathbf{y}_0, \end{aligned} \tag{42}$$

where

$$\mathbf{W}_1 = \left[\frac{2}{\Delta t} m \;\; 0 \right], \qquad \mathbf{W}_2 = \left[-\frac{3}{\Delta t} m \;\; \frac{1}{\Delta t} m \right]. \tag{43}$$

The second row of matrix $\mathbf{Q}$ represents the first row of amplification matrix, whilst the row vector $\mathbf{W}_1 + \mathbf{W}_2\mathbf{Q}$ represents the second row of $\mathbf{A}$. As a result, the amplification matrix can be obtained as

$$\mathbf{A} = \begin{bmatrix} 0 & 1 \\ 0 & 0 \end{bmatrix} \mathbf{Q} + \begin{bmatrix} 0 \\ 1 \end{bmatrix} (\mathbf{W}_1 + \mathbf{W}_2 \mathbf{Q}). \tag{44}$$

4.3. CONSISTENCY

The consistency of the new schemes can be determined from the local truncation error

$$\tau = \mathbf{y}_1 - \mathbf{y}_{ex}(\Delta t) = (\mathbf{A} - \mathbf{A}_{ex})\mathbf{y}_0, \tag{45}$$

where

$$\mathbf{A}_{ex} = \begin{bmatrix} \cos\Omega & \dfrac{\sin\Omega}{m\omega} \\ -m\omega\sin\Omega & \cos\Omega \end{bmatrix} \tag{46}$$

is the amplification matrix of the exact solution, whilst $\mathbf{y}_0$ is the exact solution at time t_i. An algorithm is said to be consistent if two positive constants C_2 and k exist such that

$$|\tau(t)| \leqslant C_2 \Delta t^{k+1}, \quad t \in [0, T], \tag{47}$$

where k is the so-called order of accuracy [1, p. 468].

The local truncation error of the E-1C scheme ($k_{max} = 1$) can be evaluated using equations (38) and (40). As a result, an accuracy of second order is obtained. The coefficient of Δt^3 in the Taylor series expansion of the local truncation error in the momenta must vanish. This constraint provides the condition

$$a = \tfrac{1}{3} - b. \tag{48}$$

Thereby, only one free parameter b is available to control the dissipative properties of the algorithms.

Besides the local truncation error, other measures of accuracy linked to the amplification matrix $\mathbf{A}$ defined in equation (44) are the algorithmic dispersion, namely the phase error, and the dissipation, namely the amplitude error. Provided that the eigenvalues of $\mathbf{A}$ remain complex, they can be expressed as

$$\lambda_{1,2} = \mathrm{e}^{\bar{\Omega}(-\bar{\xi} \pm i)}, \tag{49}$$

where $\bar{\Omega}$ and $\bar{\xi}$ are the so-called algorithmic frequency and algorithmic damping ratio respectively. The relative period error $\bar{T} - T/T = (\Omega/\bar{\Omega}) - 1$ is a measure of the phase error whilst $\bar{\xi}$ is a measure of the amplitude error. The Taylor expansions of τ, $\bar{T} - T/T$ and $\bar{\xi}$ about $\Omega = 0$ up to the leading terms are reported in Table 1 where the following notation is used:

$$\tau = \begin{bmatrix} c_q \Omega^{k_q} + O(\Omega^{k_q+1}) \\ c_p \Omega^{k_p} + O(\Omega^{k_p+1}) \end{bmatrix}, \qquad \frac{\bar{\Omega}}{\Omega} - 1 = c_{rpe}\Omega^{k_{rpe}} + O(\Omega^{k_{rpe}+1}),$$

$$\bar{\xi} = c_{adr}\Omega^{k_{adr}} + O(\Omega^{k_{adr}+1}). \tag{50}$$

From, Table 1, it is evident that both the E-1C and the E-2C schemes are third order accurate. Moreover, the E-2C scheme is endowed with the same truncation error and

TABLE 1

Accuracy properties of the TDG1 Explicit method with 1 and 2 corrector passes

Scheme	c_q	k_q	c_p	k_p	c_{rpe}	k_{rpe}	c_{adr}	k_{adr}
E-1C	$\left(\frac{5}{72}-\frac{1}{6}b\right)q_0$	4	$-\frac{1}{24}p_0$	4	$\frac{1}{45}-\frac{1}{12}b$	4	$\frac{6b-1}{72}$	3
E-2C	$-\frac{1}{72}q_0$	4	$-\frac{1}{72}p_0$	4	$\frac{1}{18}b-\frac{13}{540}$	4	$\frac{1}{72}$	3

algorithmic damping ratio of the implicit parent TDG1 algorithm presented in section 2, independent for predictor form (26). Conversely, all the remaining properties depend on the value of the free parameter b.

4.4. STABILITY

Considering the undamped case and combining equation (44) with equations (26) and (48), the following amplification matrices

$$\mathbf{A}=\begin{bmatrix}\dfrac{18-9\,\Omega^2+(2-3b)\Omega^4}{18} & \dfrac{\Delta t}{m}\left(1-\dfrac{\Omega^2}{6}\right)\\ \dfrac{m\Omega^2(-6+\Omega^2)}{6\Delta t} & 1-\dfrac{\Omega^2}{2}\end{bmatrix}, \tag{51}$$

$$\mathbf{A}=\begin{bmatrix}1-\dfrac{1}{2}\Omega^2+\dfrac{1}{36}\Omega^4-\dfrac{1}{81}\Omega^6+\dfrac{5}{108}\Omega^6 b & -\dfrac{1}{108}\dfrac{\Delta t}{m}(-108+18\Omega^2+\Omega^4)\\ \dfrac{1}{108}m\Omega^2\dfrac{-108+18\Omega^2-5\Omega^4+12\Omega^4 b}{\Delta t} & 1-\dfrac{1}{2}\Omega^2+\dfrac{1}{36}\Omega^4\end{bmatrix} \tag{52}$$

for the E-1C and for the E-2C schemes respectively, are obtained. The stability properties of an algorithm depend on the eigenvalues of $\mathbf{A}$ which assume the form

$$\lambda_{1,2}=e(\Omega,b)\pm\sqrt{h(\Omega,b)}. \tag{53}$$

The condition

$$h(\Omega,b)=0, \tag{54}$$

corresponds to the bifurcation limit Ω_b, i.e., $\lambda_{1,2}$ become real and distinct for $\Omega>\Omega_b$. Let ρ_b denote the spectral radius at the bifurcation limit Ω_b; Figures 2 and 3 plot the relations provided by condition (54) for the schemes E-1C and E-2C respectively. More specifically, these plots provide the value of b, which utilized in equations (48) and (26), permits a user-designed dissipation value ρ_b at the bifurcation limit to be achieved. For clarity, the aforementioned figures also report the values of b, Ω_b and Ω_{CR} corresponding to $\rho_b=0{\cdot}6$.

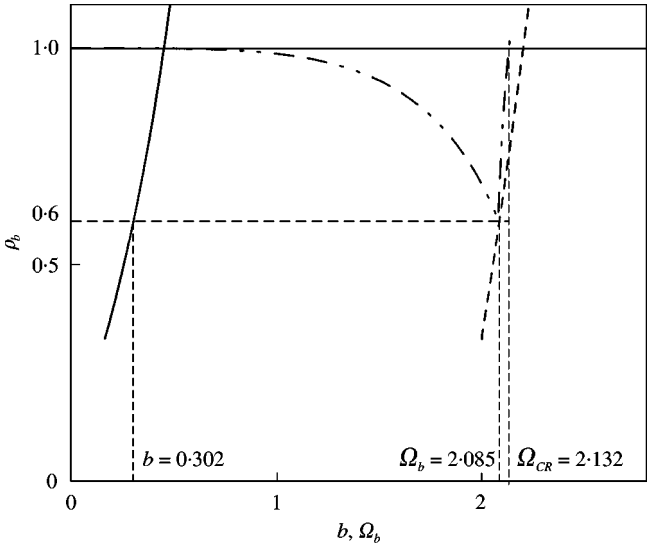

Figure 2. Relations among the spectral radius at the bifurcation limit ρ_b, the parameter b and the bifurcation limit Ω_b for the E-1C scheme (The scheme is unstable for $b < \frac{1}{6}$): ——, b; – – – – –, Ω_b.

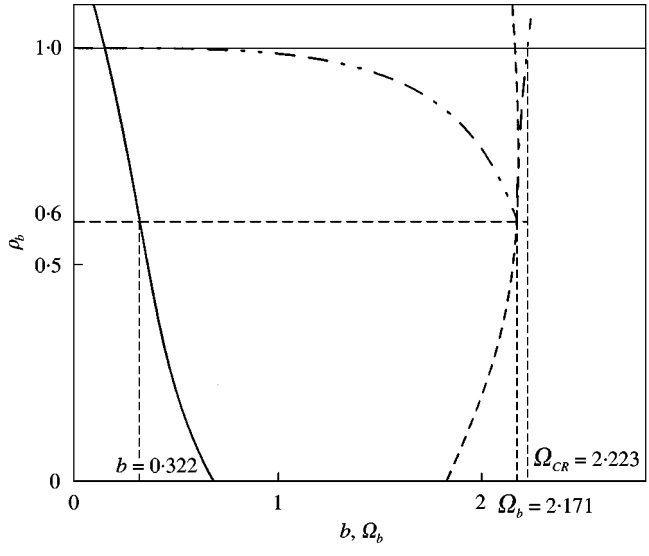

Figure 3. Relations among the spectral radius at the bifurcation limit ρ_b, the parameter b and the bifurcation limit Ω_b for the E-2C scheme: ——, b; – – – – –, Ω_b.

This leads to the values $b = 0{\cdot}302$, $\Omega_b = 2{\cdot}085$ and $\Omega_{CR} = 2{\cdot}132$ for the E-1C scheme; and $b = 0{\cdot}322$, $\Omega_b = 2{\cdot}171$ and $\Omega_{CR} = 2{\cdot}223$ for the E-2C scheme. The plots can be fitted by a third order polynomial in the design parameter ρ_b

$$b = C_{3b}\rho_b^3 + C_{2b}\rho_b^2 + C_{1b}\rho_b + C_{0b},$$

$$\Omega_b = C_{3\Omega}\rho_b^3 + C_{2\Omega}\rho_b^2 + C_{1\Omega}\rho_b + C_{0\Omega} \tag{55}$$

TABLE 2

Constants and ranges relevant to equation (55*a*)

Scheme	C_{3b}	C_{2b}	C_{1b}	C_{0b}	ρ_b range	Ω_b range	Ω_{CR} range
E-1C	0·0909	−0·3824	0·8043	−0·0622	[0·34, 1·00]	[2·00, 2·20]	[2·10, 2·20]
E-2C	−0·5624	1·0679	−1·0313	0·6776	[0·00, 1·00]	[1·83, 2·18]	[2·08, 2·69]

TABLE 3

Constants and ranges relevant to equation (55*b*)

Scheme	$C_{3\Omega}$	$C_{2\Omega}$	$C_{1\Omega}$	$C_{0\Omega}$	ρ_b range	Ω_b range	Ω_{CR} range
E-1C	0·0107	−0·064	0·3722	1·8827	[0·34, 1·00]	[2·00, 2·20]	[2·10, 2·20]
E-2C	0·2778	−1·057	1·1186	1·8199	[0·00, 1·00]	[1·83, 2·18]	[2·08, 2·69]

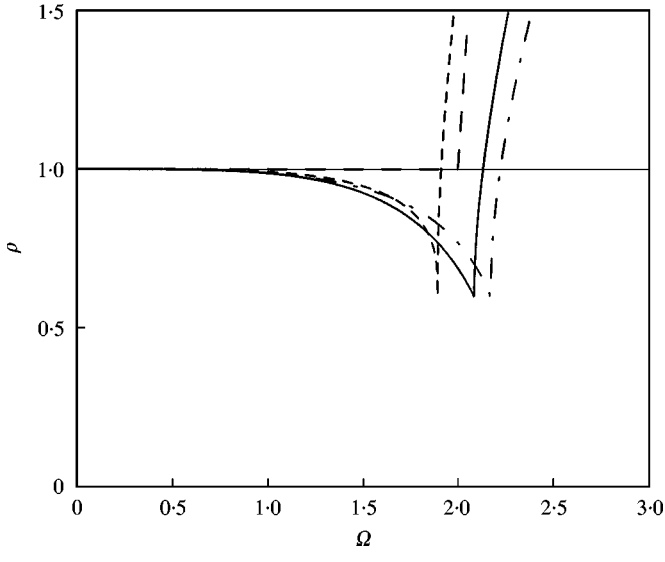

Figure 4. Spectral radii for a value at bifurcation $\rho_b = 0{\cdot}6$: ——, E-1C; —·—·, E-2C; — — —, CD; – – – – –, HCE-α.

providing explicit relations for b and Ω_b versus ρ_b. The relevant coefficients and ranges are collected in Tables 2 and 3 respectively. From these tables and Figures 2 and 3, it is evident that only the algorithm E-2C covers the entire design range [0·00, 1·00] for ρ_b. Conversely, the algorithm E-1C is unstable for $\rho_b < 0{\cdot}334$ ($b < \frac{1}{6}$).

The spectral radius ρ, the relative period error $\bar{T} - T/T$ and the algorithmic damping ratio $\bar{\xi}$ versus the non-dimensional frequency Ω are plotted in Figures 4–6 respectively. Additionally, the condition with $\rho_b = 0{\cdot}6$ is considered. For completeness, the aforementioned schemes are compared with the HCE-α method [4] that employs the same ρ_b value and with the CD scheme respectively. Besides the higher values of the stability limits Ω_{CR} of the proposed methods shown in Figure 4, the favourable accuracy properties are evident.

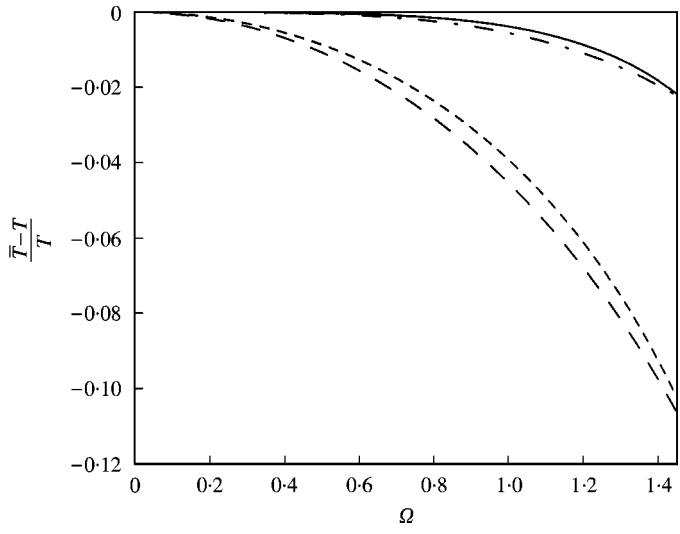

Figure 5. Relative period errors for a value at bifurcation $\rho_b = 0{\cdot}6$: ——, E-1C; —·—·, E-2C; — — —, CD; – – – – –, HCE-α.

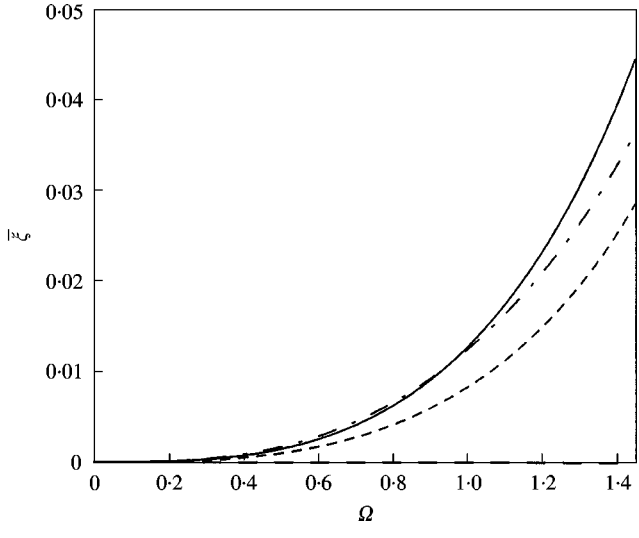

Figure 6. Algorithmic damping ratios for a value at bifurcation $\rho_b = 0{\cdot}6$: ——, E-1C; —·—·, E-2C; — — —, CD; – – – – –, HCE-α.

In order to analyze the properties of the proposed schemes as a function of the maximum number k_{max} of corrector passes, the case $k_{max} = 3$, which corresponds to the scheme E-3C has also been considered. More specifically, Figure 7 reports, among the various parameters, the spectral radius $\rho_b \in [0, 0{\cdot}45]$. Moreover, Figures 8 and 9 plot the spectral radius ρ and the relative period error $\bar{T} - T/T$ versus Ω, together with those of the schemes E-1C and E-2C for the condition $\rho_b = 0{\cdot}4$. The improved properties of the E-3C scheme may be seen in Figure 8, which exhibits higher values of $\Omega_b(= 2{\cdot}753)$ and $\Omega_{CR}(= 2{\cdot}799)$. Moreover, the satisfactory behaviour of the relative period error $\bar{T} - T/T$ of the method E-3C is evident in Figure 9. Nonetheless, as the E-2C scheme has the same local truncation

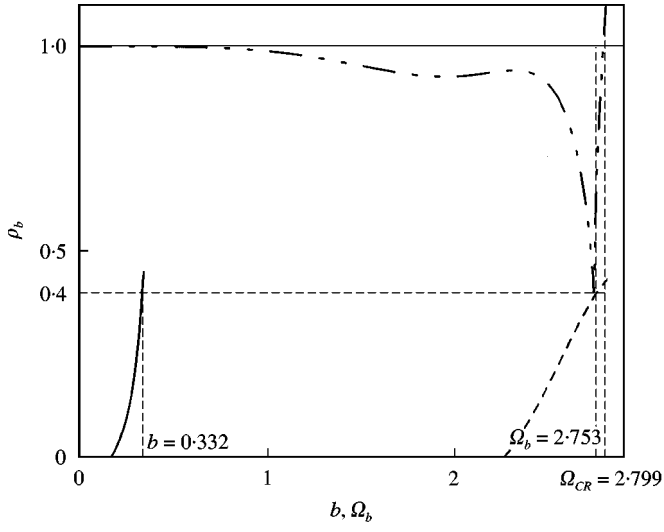

Figure 7. Relations among the spectral radius at the bifurcation limit ρ_b, the parameter b and the bifurcation limit Ω_b for the E-3C scheme: ——, b; – – – – –, Ω_b.

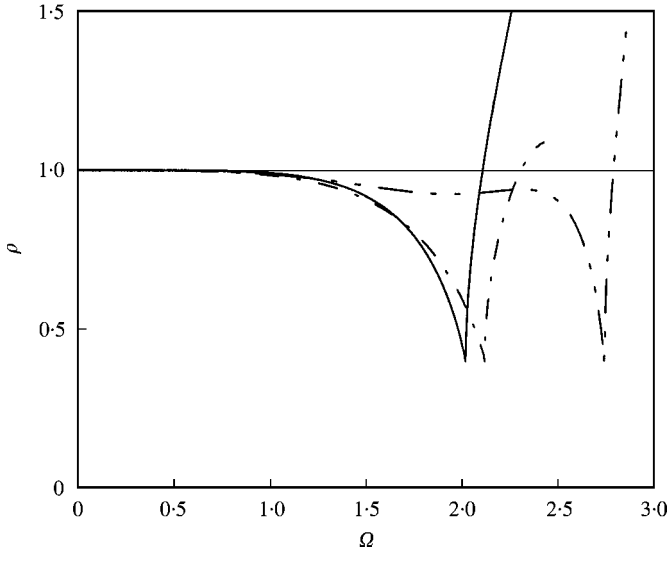

Figure 8. Spectral radii for a value at bifurcation $\rho_b = 0{\cdot}4$: ——, E-1C; —·—·, E-2C; —· ·—, E-3C.

error of the implicit parent algorithm (see Table 1), and the computational effort increases with k_{max}, the schemes relying on $k_{max} > 2$ are not considered further.

4.5. CONSISTENCY OF THE TDG EXPLICIT METHOD FOR DAMPED SYSTEMS

In the presence of damping, the equation of motion relevant to a single-degree-of-freedom system is

$$\ddot{q}(t) + 2\xi\omega\dot{q}(t) + \omega^2 q(t) = \frac{f(t)}{m} \tag{56}$$

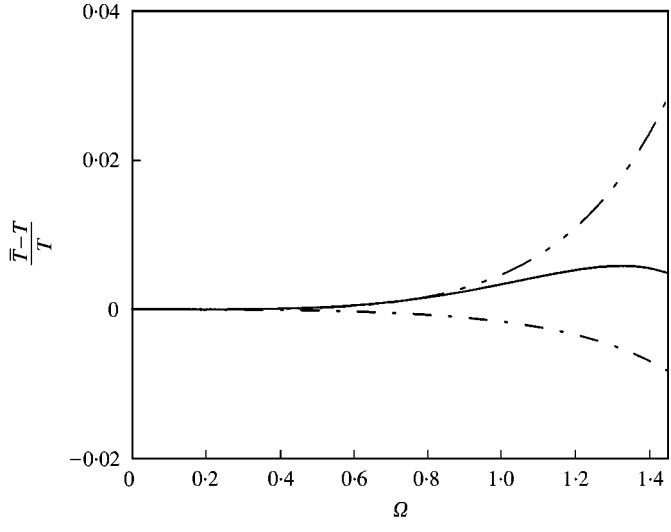

Figure 9. Relative period errors for a value at bifurcation $\rho_b = 0{\cdot}4$: ——, E-1C; —·—·, E-2C; —· ·—, E-3C.

and the time derivative of momenta becomes

$$\dot{p}_0 = f(0) - m\left(2\xi\omega\frac{p_0}{m} + \omega^2 q_0\right). \tag{57}$$

In order to evaluate the local truncation error τ, the exact amplification matrix $\mathbf{A}_{ex}$ is needed, which for an underdamped system is expressed as

$$\mathbf{A}_{ex} = \mathrm{e}^{-\xi\Omega}\begin{bmatrix} \cos(v\Omega) + \dfrac{\xi\sin(v\Omega)}{v} & \dfrac{\sin(v\Omega)}{mv\omega} \\ -m\omega\dfrac{\sin(v\Omega)}{v} & -\dfrac{\xi\sin(v\Omega)}{v} + \cos(v\Omega) \end{bmatrix}, \tag{58}$$

where

$$v = \sqrt{(1-\xi^2)}. \tag{59}$$

The local truncation error τ can be evaluated through the predictor defined in equation (38) and one corrector of equation (40). As illustrated in section 3.3, the damping can be dealt with either implicitly or explicitly.

When an implicit damping treatment is utilized for the E-1C scheme, τ is

$$\tau = \begin{bmatrix} \left(\dfrac{-1+3b+6a+\xi^2}{9m}\,\xi p_0 + \dfrac{12b+24a+4\xi^2-3}{72}\,\omega q_0\right)\omega^3\Delta t^4 + O(\Delta t^5) \\ \dfrac{1}{6}\omega^3(3b+3a-1)(2\xi p_0 + \omega q_0 m)\Delta t^3 + O(\Delta t^4) \end{bmatrix}. \tag{60}$$

If relation (48) is exploited in equation (60), an accuracy of third order is attained.

Conversely, the local truncation error τ of the E-1C scheme formulated with an explicit damping treatment becomes

$$\tau = \begin{bmatrix} \frac{1}{3}\omega^2\xi(3b + 3a - 1)\left(\frac{2}{m}\xi p_0 + \omega q_0\right)\Delta t^3 + O(\Delta t^4) \\ \omega^2\xi(2b - 1)(2\xi p_0 + \omega q_0 m)\Delta t^2 + O(\Delta t^3) \end{bmatrix}. \tag{61}$$

From equation (61) it may be observed that the explicit damping treatment entails only a first order accurate scheme. A second order accuracy is achieved if

$$b = \tfrac{1}{2}. \tag{62}$$

These results agree with the behaviour of other explicit predictor–corrector Newmark methods [14], [1, p. 562].

With regard to the E-2C scheme, the local truncation error is

$$\tau = \begin{bmatrix} -\dfrac{\omega q_0 m + 192a\xi^3 p_0 + 4\xi p_0 + 96a\xi^2\omega q_0 m + 96b\xi^3 p_0 + 48b\xi^3\omega q_0 m - 12\xi^2\omega q_0 m - 24\xi^3 p_0}{72m}\omega^3\Delta^4 + O(\Delta^5) \\ -\dfrac{2}{3}\omega^3\xi^2(3b + 3a - 1)(2\xi p_0 + \omega q_0 m)\Delta^3 + O(\Delta^4) \end{bmatrix}. \tag{63}$$

In addition, a third order accuracy can be obtained when relation (48) is exploited.

5. REPRESENTATIVE NUMERICAL SIMULATIONS

In this section, two representative numerical examples are introduced both to evaluate the performance of the new class of time-step algorithms and to warrant the analytical findings obtained so far. To this end, a linear two-degrees-of-freedom system endowed with natural frequencies typical of large systems is introduced [1, p. 542], in order to highlight the favourable accuracy and dissipative properties of higher modes of the proposed schemes. The second problem deals with the impact of a linear elastic rod on a rigid wall, representative of a wave propagation problem [4]. Since the discontinuity in the velocity and strain (weak shocks) influences the physical solution, high-frequency dissipation of spurious responses is a desired feature.

5.1. TWO-DEGREES-OF-FREEDOM SYSTEM

The following system of differential equations is considered:

$$\mathbf{M}\ddot{\mathbf{q}}(t) + \mathbf{K}\mathbf{q}(t) = \mathbf{0}, \tag{64}$$

where

$$\mathbf{M} = \begin{bmatrix} m_1 & 0 \\ 0 & m_2 \end{bmatrix}, \quad \mathbf{K} = \begin{bmatrix} k_1 + k_2 & -k_2 \\ -k_2 & k_2 \end{bmatrix},$$

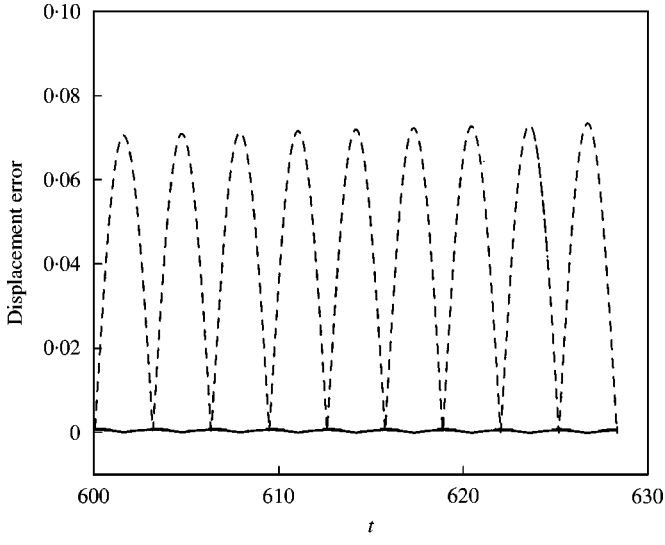

Figure 10. Displacement error of q_2 versus time for the fundamental mode: ——, E-1C; —·—·, E-2C; – – – – –, HCE-α.

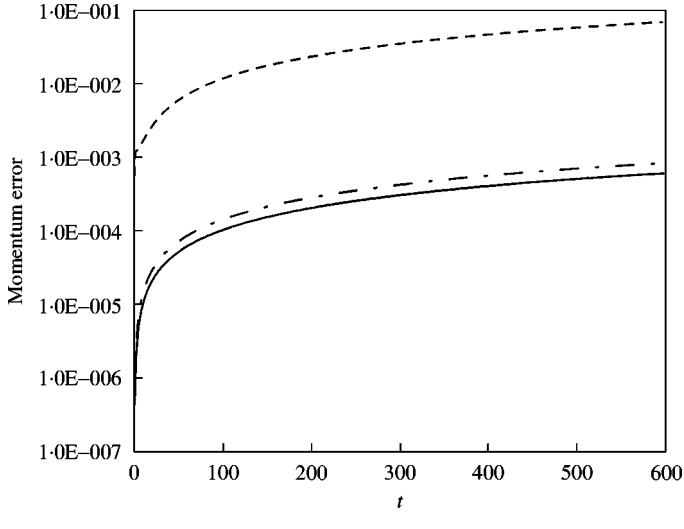

Figure 11. Evolution of local maxima errors of p_2 for the fundamental mode: ——, E-1C; —·—·, E-2C; – – – – –, HCE-α.

$k_1 = 10^4$, $k_2 = 1$ and $m_1 = m_2 = 1$. The assumed initial conditions are

$$\mathbf{q}_0 = \begin{Bmatrix} 1 \\ 10 \end{Bmatrix} \quad \text{and} \quad \mathbf{p}_0 = \begin{Bmatrix} 0 \\ 0 \end{Bmatrix} \tag{65}$$

[1, p. 542]. The two natural frequencies of the system are

$$\omega_1 = 0{\cdot}99995 \quad \text{and} \quad \omega_2 = 100{\cdot}005. \tag{66}$$

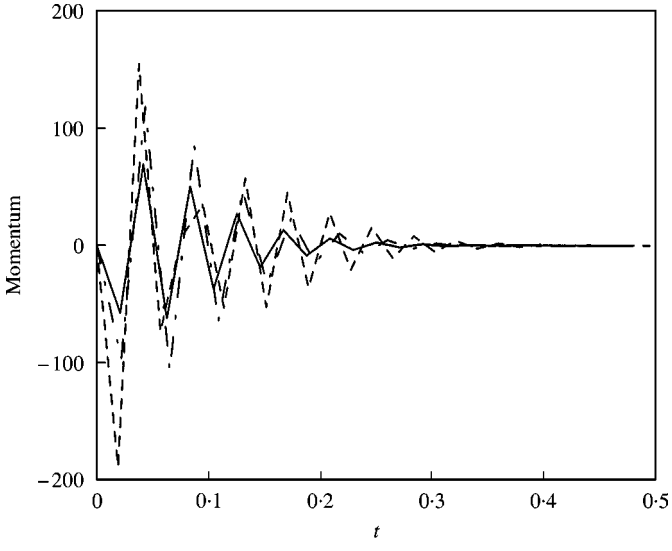

Figure 12. Evolution of p_2 versus time for the spurious mode: ——, E-1C; —·—·, E-2C; – – – – –, HCE-α.

The mode related to the lower frequency represents those modes that are physically important and must be accurately integrated. The second mode represents those spurious high-frequency modes which have to be filtered by the numerical method. A fixed time step $\Delta t = \Omega_b/\omega_2$ is chosen in order to integrate the high-frequency mode at the bifurcation limit with a spectral radius $\rho_b = 0{\cdot}6$. The integration has been performed over $100T_1$ wereT_i denotes the period relative to the natural frequency $\omega_i = 2\pi/T_i$. The exact solutions being available, both the displacement error $|q_{ex}(t_{i+1}) - q_{2,(i+1)}|$ and the momentum error $|p_{ex}(t_{i+1}) - p_{2,(i+1)}|$ can be computed for each degree-of-freedom.

The results provided by the E-1C and E-2C schemes are compared with those obtained by means of the HCE-α method [4] in Figures 10–12. In detail, Figure 10 highlights the displacement error at the end of each time step for the response of the fundamental mode whilst Figure 11 presents the momentum error related to the local maxima. The satisfactory performance of the proposed schemes is evident. Moreover, it may be observed from Figure 11 that the algorithm E-1C exhibits a smaller momentum error than the one shown by the E-2C scheme. The behaviour is caused by two factors: (i) the E-1C scheme is endowed with a lower bifurcation limit Ω_b and thereby a smaller time step has been used; (ii) the E-1C method exhibits both a lower relative period error $\bar{T} - T/T$ and a lower algorithmic damping ratio on $\bar{\xi}$ for a spectral radius $\rho_b = 0{\cdot}6$ as illustrated in Figures 5 and 6, respectively. The filtering of the spurious response is highlighted in Figure 12, where the relevant evolution of the momentum at the end of each time step is plotted.

5.2. IMPACT OF A TAPERED ROD

The second example deals with a one-dimensional model of a rod impacting a rigid wall. This problem has been proposed in the literature as spurious oscillations that arise when non-dissipative integrators like the Constant Average Acceleration and the CD method are adopted [4, 15]. The problem is sketched in Figure 13 where a homogeneous elastic rod with a varying cross-sectional area and an initial uniform velocity $v_0 = 1$ is considered [4].

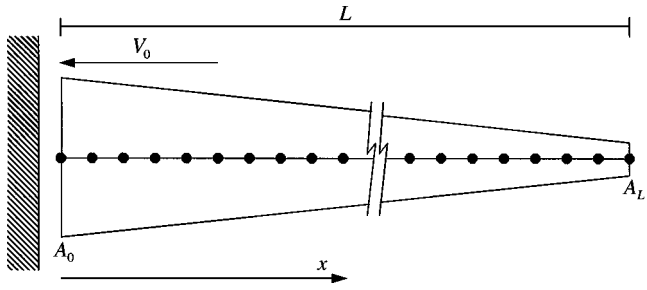

Figure 13. A tapered rod impacting on a rigid wall.

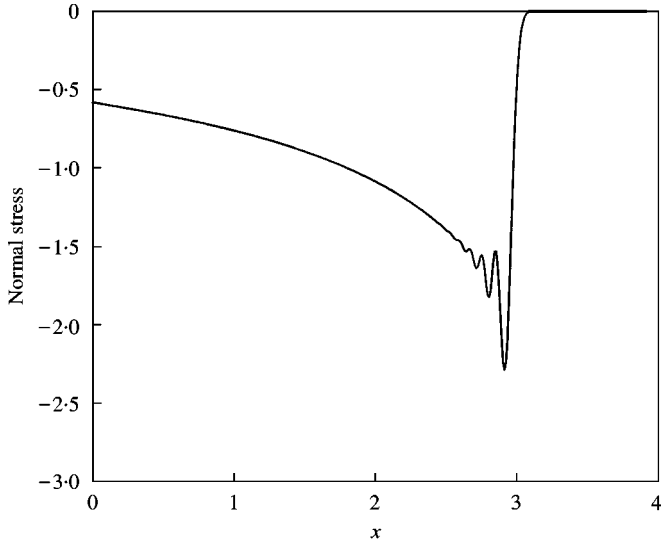

Figure 14. Stress distribution in the tapered rod at time $t = 3$ predicted by the E-2C scheme with $\rho_b = 0{\cdot}6$.

The length L of the rod is equal to 4, the density ρ and Young's modulus E have unit values whilst the cross-sectional areas are assumed to be $A_0 = 1$ and $A_L = 0{\cdot}01$ respectively.

The governing equation of the problem is

$$\frac{\partial}{\partial x}\left(EA\frac{\partial u}{\partial x}\right) - \rho A\ddot{u} = 0 \tag{67}$$

with the boundary conditions

$$u(0, t) = 0 \text{ and } EA\left.\frac{\partial u}{\partial x}\right|_{x=L} = 0 \tag{68}$$

and the initial conditions defined above. The exact solution consists of a stress front propagating along the rod with the elastic wave speed $c = \sqrt{E/\rho} = 1$. With linear rod elements, the maximum element eigenfrequency that represents an upper bound of the

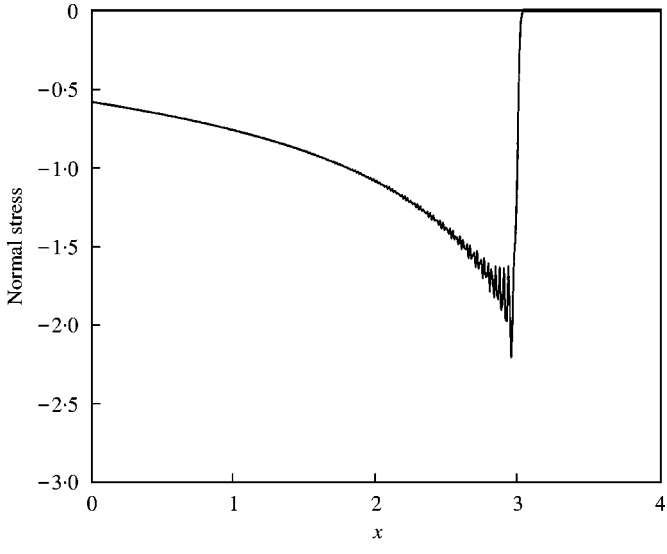

Figure 15. Stress distribution in the tapered rod at time $t = 3$ predicted by the CD method.

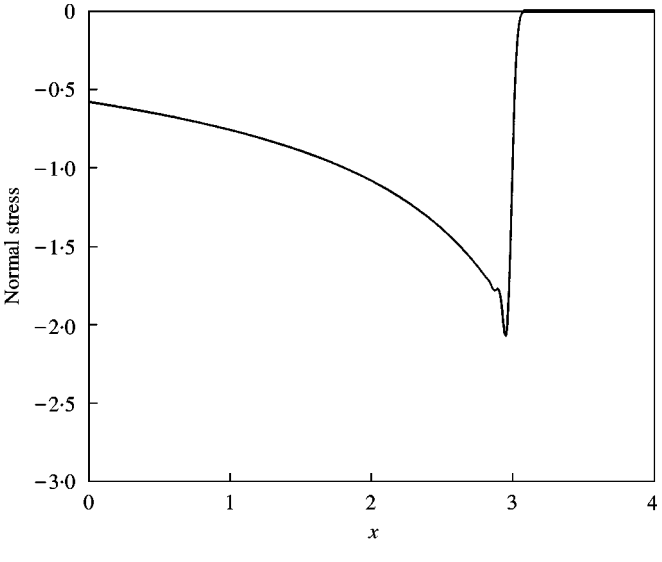

Figure 16. Stress distribution in the tapered rod at time $t = 3$ predicted by the HCE-α method with $\rho_b = 0{\cdot}6$.

maximum structure eigenfrequency is given by

$$\omega^e_{max} = \frac{c(A_i + A_{i+1})}{l^e\sqrt{A_i A_{i+1}}}. \tag{69}$$

The system is discretized with 400 elements and has been integrated with the E-2C scheme, the CD and the HCE-α method respectively. In addition, a fixed time step $\Delta t = \Omega_b/\omega^e_{max}$ is chosen in order to integrate the high-frequency modes at the bifurcation limit with a spectral radius $\rho_b = 0{\cdot}6$. Figures 14–16 highlight spurious oscillations of the stress distribution exhibited by the CD method which is undermined by the lack of algorithmic

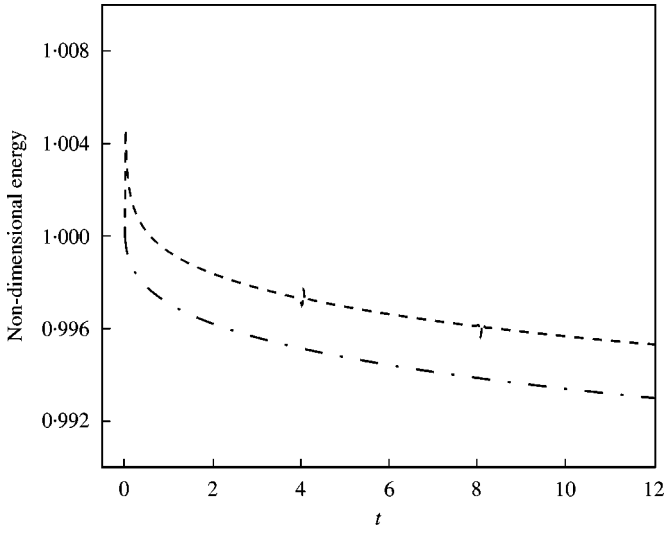

Figure 17. Time history of the energy predicted by the E-2C and HCE-α methods with $\rho_b = 0{\cdot}6$: —·—·, E-2C; – – – – –, HCE-α.

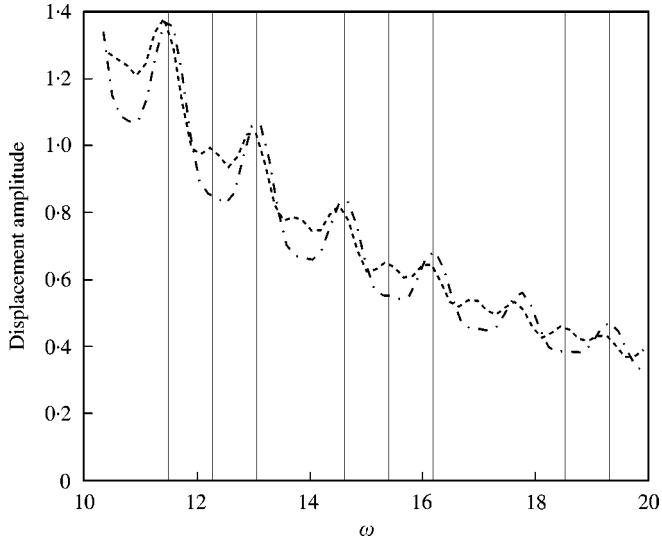

Figure 18. Displacement FFT at the rod midpoint with the frequencies of the discretized tapered rod: —·—·, E-2C; – – – – –, HCE-α; ——, ω_i.

damping, and the limited oscillations relevant to the dissipative schemes. Figure 17 plots the energy evolution up to $t = 12$. As expected, the HCE-α method exhibits the overshoot phenomenon in the first step, typical of the α-methods [16, p. 134]. Moreover, spurious oscillations are evident at every 4 s when the wave front reaches the rod ends. Conversely, the E-2C scheme does not exhibit this unfavourable behaviour.

Figure 18 illustrates the frequency content of the responses at the rod midpoint, provided by the FFT transform of the time history between $t = 0$ and 12·0 whilst vertical lines identify the frequencies of the discretized rod. The frequency resolution is 0·154 rad/s for the response of the E-2C scheme and 0·163 rad/s for the response of the HCE-α method

respectively. Hanning windowing was adopted to reduce the time domain truncation effects [17, p. 140]. One can observe easily that the E-2C scheme is also to approximate accurately the frequency content of the discretized rod owing to better amplitude and phase error properties.

6. CONCLUDING REMARKS

The formulation of a new class of explicit Time Discontinuous Galerkin methods has been presented in the paper. The algorithms derive directly from the implicit parent TDG method with piecewise linear functions in time, which approximate displacements and momenta. In order to avoid an expensive explicit formulation, the proposed schemes are implemented in an explicit predictor–multicorrector form with one and two corrector passes. Accuracy and stability analyses have been performed on undamped systems showing that the schemes are third order accurate and can be adopted with a user-defined dissipation, and are helpful in eliminating unresolved non-physical high-frequency modes in the time response. Moreover, the dissipative properties of the schemes are achieved without introducing any spurious root as only displacements and momenta are involved in the formulation. The analyses have been extended to damped systems considering both an explicit and an implicit damping treatment. Numerical simulations have shown the importance of the accuracy and of the dissipative properties of the explicit Time Discontinuous Galerkin schemes when compared to those of standard finite-difference-based methods. These properties render the new proposed methods competitive for medium-term high-quality analyses.

ACKNOWLEDGMENT

The financial support from the Italian Ministry for Universities and Scientific and Technological Research (MURST) is acknowledged.

REFERENCES

1. T. J. R. HUGHES 1987 *The Finite Element Method, Linear Static and Dynamic Finite Element Analysis*. Englewood Cliffs, NJ: Prentice-Hall.
2. M. G. KATONA and O. C. ZIENKIEWICZ 1985 *International Journal for Numerical Methods in Engineering* **21**, 1345–1359. A unified set of single-step algorithms. Part 3: The β-m method. A generalization of the Newmark scheme.
3. C. HOFF and R. L. TAYLOR 1990 *International Journal for Numerical Methods in Engineering* **29**, 275–290. Higher derivative explicit one step methods for non-linear dynamic problems. Part I: Design and theory.
4. G. M. HULBERT and J. CHUNG 1996 *Computer Methods in Applied Mechanics and Engineering* **137**, 175–188. Explicit time integration algorithms for structural dynamics with optimal numerical dissipation.
5. G. M. HULBERT 1994 *Computer Methods in Applied Mechanics and Engineering* **113**, 1–9. A unified set of single step asymptotic annihilation algorithms for structural dynamics.
6. M. BORRI and C. BOTTASSO 1993 *Computational Mechanics* **13**, 133–142. A general framework for interpreting time finite element formulations.
7. M. CANNAROZZI and M. MANCUSO 1995 *Computer Methods in Applied Mechanics and Engineering* **127**, 241–257. Formulation and analysis of variational methods for time integration of linear elastodynamics.
8. T. C. FUNG and A. Y. T. LEUNG 1996 *Journal of Vibration and Control*, 193–217. On the accuracy of discontinuous Galerkin methods in the time domains.

9. X. D. LI and N. E. WIBERG 1996 *International Journal for Numerical Methods in Engineering* **39**, 2131–2152. Structural dynamics analysis by a time-discontinuous Galerkin finite element method.
10. N. E. WIBERG and X. D. LI 1997 in *Proceedings of COMPLAS V*: *Computational Plasticity, Fundamentals and Applications* (D. R. J. Owen, E. Onate, and E. Hinton, editors) 224–237, Barcellona: CIMNE. Implicit and explicit discontinuous Galerkin finite element procedures for linear and nonlinear structural dynamic analysis.
11. N. E. WIBERG and X. D. LI 1999 *International Journal for Numerical Methods in Engineering* **46**, 1781–1802. Adaptive finite element procedures for linear and non-linear dynamics.
12. K. K. TAMMA and R. R. NAMBURU 1990 *International Journal for Numerical Methods in Engineering* **29**, 1441–1454. A robust self-starting explicit computational methodology for structural dynamic applications: Architecture and representations.
13. C. T. KELLEY 1995 *Iterative Methods for Linear and Nonlinear Equations*. Philadelphia, PA: SIAM.
14. I. MIRANDA, R. M. FERENCZ and T. J. R. HUGHES 1989 *Earthquake Engineering and Structural Dynamics* **18**, 643–653. An improved implicit–explicit time integration method for structural dynamics.
15. T. J. R. HUGHES and W. K. LIU 1978 *Journal of Applied Mechanics* **45**, 375–378. Implicit–explicit finite elements in transient analysis: implementation and numerical examples.
16. W. L. WOOD 1990 *Practical Time-Stepping Schemes*. Oxford: Clarendon Press.
17. E. O. BRIGHAM 1988 *The Fast Fourier Transform and its Application*. Englewood Cliffs, NJ: Prentice-Hall Signal Proceeding Series.
18. H. M. HILBER and T. J. R. HUGHES 1978 *Earthquake Engineering and Structural Dynamics* **6**, 99–117. Collocation, dissipation and "overshoot" for time integration schemes in structural dynamics.

APPENDIX A

The displacement predictor defined in equation (16) needs the computation of the acceleration vector $\mathbf{M}^{-1}\dot{\mathbf{p}}$. In this appendix, the new proposed schemes are formulated with an efficient alternative computation of the vector $\mathbf{M}^{-1}\dot{\mathbf{p}}$, based on the derivative of the momentum time interpolants. In order to establish the effectiveness of this alternative approach, an accuracy and stability analysis of the methods is performed.

The algorithms proposed in section 3 are based on equation (15). Nonetheless from a computational standpoint, the computation of $\mathbf{M}^{-1}\dot{\mathbf{p}}$ is convenient as a derivative of the momentum field, namely

$$\begin{aligned}\mathbf{M}^{-1}\dot{\mathbf{p}}(t+\Delta t) &= \mathbf{M}^{-1}(\dot{t}_1(t+\Delta t)\mathbf{p}_1 + \dot{t}_2(t+\Delta t)\mathbf{p}_2)\\ &= \mathbf{M}^{-1}\frac{\mathbf{p}_2-\mathbf{p}_1}{\Delta t} = \frac{6}{\Delta t^2}(-\mathbf{q}_1+\mathbf{q}_0).\end{aligned} \tag{A1}$$

The vector $\mathbf{M}^{-1}\dot{\mathbf{p}}(t+\Delta t)$, being a function of the time discontinuity, needs to be initialized from the equilibrium equation at the first step. Thereby, the schemes become one-step three-stage methods which can be analyzed as linear multistep methods. With regard to the E-1C scheme, on the basis of equation (16) the so-called amplification matrix $\mathbf{A}$ is

$$\mathbf{A} = \begin{bmatrix} 1-\frac{1}{2}\Omega^2 & \frac{1}{m}\left(\Delta t - \frac{1}{6}\Delta t\Omega^2\right) & -\frac{1}{6}(2a+b)\Delta t^2\Omega^2 \\ -\frac{1}{\Delta t}\Omega^2 m & 1-\frac{1}{2}\Omega^2 & -\frac{1}{2}(a+b)\Delta t\Omega^2 m \\ -\frac{\Omega^2}{\Delta t^2} & -\frac{2}{3\Delta t}\frac{\Omega^2}{m} & -\frac{1}{3}(a+2b)\Omega^2 \end{bmatrix}, \tag{A2}$$

where the undamped case is considered. The local truncation error can also be defined as

$$\tau = \frac{[q(t+\Delta t) + A_2 q(t) + A_1 q(t-\Delta t) + A_0 q(t-2\Delta t)]}{\Delta t^2}, \tag{A3}$$

where A_2, A_1 and A_0 are coefficients of the characteristic polynomial associated with **A** [18]. The order of accuracy is the order of the lowest term of the Taylor power series expansion of equation (72). As a result,

$$\tau = \frac{1}{6}\omega^4 d(3a+3b-1)\Delta t^2 - \frac{1}{12}\omega^4 \frac{p_0}{m}(4a+6b-1)\Delta t^3 + O(\Delta t^4) \tag{A4}$$

which implies that the scheme is second order accurate. Third order accuracy can be attained provided that

$$3a + 3b - 1 = 0. \tag{A5}$$

Anew, the condition established through equation (48) is obtained. As a result, the use of equation (70) does not modify the accuracy order of the algorithm. Inserting equation (48) in equation (16), the amplification matrix reads

$$\mathbf{A} = \begin{bmatrix} 1 - \frac{1}{2}\Omega^2 & \frac{\Delta t}{m} - \frac{1}{6}\Delta t \frac{\Omega^2}{m} & \frac{-2+3b}{18}\Delta t^2 \Omega^2 \\ -\frac{1}{\Delta t}\Omega^2 m & 1 - \frac{1}{2}\Omega^2 & -\frac{1}{6}\Delta t \Omega^2 m \\ -\frac{\Omega^2}{\Delta t^2} & -\frac{2}{3\Delta t}\frac{\Omega^2}{m} & -\frac{1+3b}{9}\Omega^2 \end{bmatrix} \tag{A6}$$

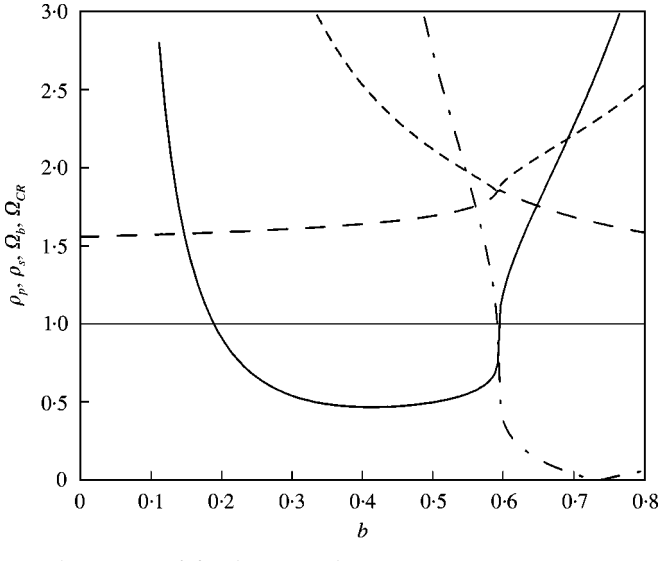

Figure A1. ρ_b, ρ_s, Ω_b and Ω_{CR} versus b for the E-1C scheme: ——, ρ_p; —·—·, ρ_s; — — —, Ω_b; - - - - -, Ω_{CR}.

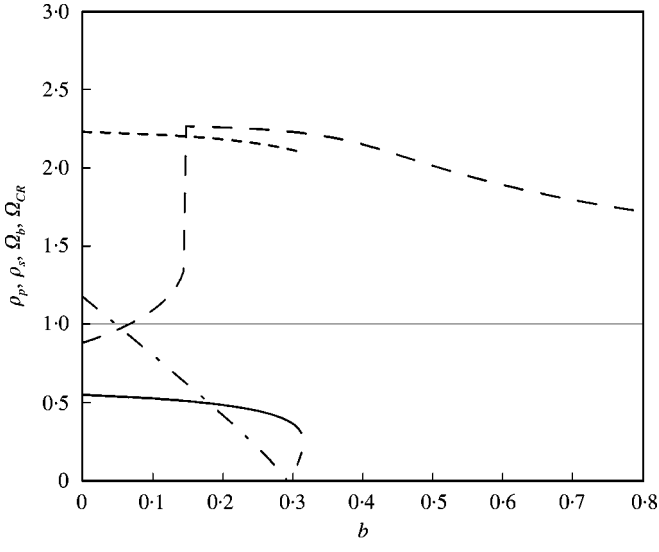

Figure A2. ρ_b, ρ_s, Ω_b and Ω_{CR} versus b for the E-2C scheme: ——, ρ_p; —·—·, ρ_s; — — —, Ω_b; - - - - -, Ω_{CR}.

for the E-1C scheme, and

$$\mathbf{A} = \begin{bmatrix} 1 - \frac{1}{2}\Omega^2 + \frac{1}{36}\Omega^4 & \frac{\Delta t - \frac{1}{6}\Delta t\Omega^2 - \frac{1}{108}\Delta t\Omega^4}{m} & \frac{4-15b}{324}\Delta t^2\Omega^4 \\ \frac{-6+\Omega^2}{6\Delta t}\Omega^2 m & 1 - \frac{1}{2}\Omega^2 + \frac{1}{36}\Omega^4 & \frac{5-12b}{108} m\Delta t\Omega^4 \\ \frac{-18+5\Omega^2}{18}\frac{\Omega^2}{\Delta t^2} & \frac{2}{27}\frac{\Omega^2-9}{\Delta t m}\Omega^2 & -\frac{11+21b}{162}\Omega^4 \end{bmatrix} \tag{A7}$$

for the E-2C scheme respectively.

These matrices lead to stability regions and dissipation properties which differ from those obtained in section 4, owing to the introduction of a spurious root. More specifically, define ρ_p as the modulus of the two complex conjugate principal roots at the bifurcation limit Ω_b, and ρ_s as the modulus of the spurious root at the same limit. The values of ρ_p, ρ_s, Ω_b and Ω_{CR} versus the free parameter b are plotted in Figures A1 and A2 for the E-1C and the E-2C schemes respectively. It can be seen that the spurious root has a modulus higher than that of the principal roots, namely $\rho_p < \rho_s$ for different values of b. As a result, $\Omega_{CR} < \Omega_b$ and the high-frequency numerical dissipation is not maximized by the schemes [4]. Moreover, as highlighted in Figure 20, the E-2C method has no bifurcation limit Ω_b for $b > 0{\cdot}31$, the principal roots always being complex conjugate. Summing up, the new proposed algorithms cannot exhibit favourable high-frequency numerical dissipation properties if formulated through equation (A1).